Available online at www.sciencedirect.com

SciVerse ScienceDirect

Ceramics International 39 (2013) 2811–2819

CERAMICS INTERNATIONAL

www.elsevier.com/locate/ceramint

Optical and photocatalytic properties of La-doped ZnO nanoparticles prepared via precipitation and mechanical milling method

Sumetha Suwanboon[a,e,*], Pongsaton Amornpitoksuk[b,e], Apinya Sukolrat[c], Nantakan Muensit[d,e]

[a]*Department of Materials Science and Technology, Faculty of Science, Prince of Songkla University, Hat Yai, Songkhla 90112, Thailand*
[b]*Department of Chemistry and Center of Excellence for Innovation in Chemistry, Faculty of Science, Prince of Songkla University, Hat Yai, Songkhla 90112, Thailand*
[c]*Scientific Equipment Center, Prince of Songkla University, Hat Yai, Songkhla 90112, Thailand*
[d]*Department of Physics, Faculty of Science, Prince of Songkla University, Hat Yai, Songkhla 90112, Thailand*
[e]*Center of Excellence in Nanotechnology for Energy (CENE), Prince of Songkla University, Hat Yai, Songkhla 90112, Thailand*

Received 29 July 2012; received in revised form 14 September 2012; accepted 14 September 2012
Available online 24 September 2012

Abstract

The synthetic method used for preparing ZnO nanoparticles strongly influenced the products obtained. The ZnO powders incorporated more La when prepared by the mechanical milling method whereas the La_2O_3/ZnO composite nanoparticles were formed better using the precipitation method. The phase formations were detected by the X-ray diffraction technique and the morphology of the samples was followed by scanning electron microscopy. The La contents affected the crystallite size. This was explained by the formation of La–O–Zn on the surface of the samples and by the Zener pinning effect. The band gap energy of the samples was influenced by repulsion between the valence and conduction bands and the presence of a secondary phase. The photocatalytic degradation of a methylene blue solution by the samples depended upon the number of oxygen vacancies.

Keywords: A. Milling; A. Powders: Chemical precipitation; C. Optical properties; D. ZnO

1. Introduction

Zinc oxide (ZnO) is an important semiconductor material both in the form of a ceramic or a powder. Intrinsically, ZnO is an n-type semiconducting compound with a wide band gap energy of about 3.2 eV and a large exciton binding energy of 60 meV at room temperature [1]. Due to its unique properties, ZnO can be used for many applications including the production of paint [2], ceramics [3], photocatalysis [4] and electronics [5]. For a decade now, photocatalytic studies have mainly focused on TiO_2 [6–8] because it is a stable and harmless material. However, TiO_2 particles have to be excited by high photon energy to initiate any photocatalytic process. This catalyst has a low quantum yield rate due to its low rate of electron transfer to oxygen and so allows for a high rate of recombination of excited electrons and holes [9]. Recently, many research groups have concentrated on the potential of ZnO particles for their photocatalytic activities instead of TiO_2 particles. Although the band gap energy and photodegradation mechanism are similar, many documents have reported that the ZnO photocatalyst had a higher photocatalytic efficiency [10]. Moreover, ZnO, in contrast to TiO_2, can be synthesized from common inorganic zinc salts. It is well known that ZnO nanoparticles can be fabricated through two major routes, namely (1) the top-down route that includes conventional [11], mechanochemical [12] and mechanical milling [13] and (2) the bottom-up route that includes solvothermal [14], sol–gel [15] and precipitation methods [16]. Both these major routes have different advantages and disadvantages; but each can be used to

*Corresponding author at: Department of Materials Science and Technology, Faculty of Science, Prince of Songkla University, Hat Yai, Songkhla 90112, Thailand. Tel.: +66 74 28 82 50; fax: +66 74 28 83 95.
E-mail address: ssuwanboon@yahoo.com (S. Suwanboon).

0272-8842/$ - see front matter © 2012 Elsevier Ltd and Techna Group S.r.l. All rights reserved.
http://dx.doi.org/10.1016/j.ceramint.2012.09.050

produce high quality ZnO nanoparticles. In this study, the precipitation and mechanical milling methods were chosen as representatives for bottom-up and top-down techniques, respectively. For precipitation method, this is a common method that can be used for large scale production, the unsophisticated equipments are required and the morphology can be modified by addition of appropriate surfactants and doping metals [17]. For the mechanical milling technique, this method can easily reduce the particle size down to nanoscale level, the solubility limit of doping metal can be extended at low temperature and amorphous phase can be easily produced [18]. Recently, a number of studies have focused on improving the ZnO properties by doping with metals. Amornpitoksuk et al. [19] investigated the effects of Ag-doped ZnO nanoparticles, prepared by a precipitation method, on their structural, photocatalytic and antibacterial properties. They reported that the particle sizes decreased, and the photocatalytic efficiency for degradation of methylene blue increased as a function of the Ag concentration. The Ag-doped ZnO nanoparticles inhibited *Staphylococcus aureus*, but had no effect on *Escherichia coli*. Benhebal et al. [20] showed that the band gap energy was reduced when ZnO was doped with 10% lithium, sodium or potassium due to an increase in its crystallinity. The Na- and Li-doped ZnO particles also had an improved efficiency to degrade phenol and benzoic acid, but the K-doped ZnO particles had reduced degradation efficiency. He et al. [21] prepared Co-doped ZnO nanoparticles by a co-precipitation method and concluded that the photocatalytic degradation of Rhodamine B was decreased by Co-doping. Xu et al. [22] revealed the effects of changing Co concentrations on the properties of ZnO nanoparticles that had been synthesized by the hydrothermal method. They found that the crystallite size decreased and band gap energy increased as a function of the Co concentration. They also reported that the 3 mol% Co-doped ZnO nanoparticles degraded 78% of methyl orange after reacting for 240 min. Zhong et al. [23] prepared Bi-doped ZnO nanoparticles by a parallel flaw precipitation method. The 5 mol% Bi-doped ZnO nanoparticles showed a better photocatalytic degradation of methyl orange. Patil et al. [24] studied the effect of S-doped ZnO nanoparticles prepared by a mechanochemical synthesis on their structural, optical and photocatalytic properties. They concluded that the incorporation of sulfur expanded the lattice constant of the ZnO and the S-doped ZnO nanoparticles had more oxygen vacancies than pure ZnO. This produced an increase in photocatalytic efficiency. Anandan et al. [25] prepared La-doped ZnO nanoparticles by a co-precipitation method and they showed that the rate of degradation of monocrotophos in aqueous solution for La-doped ZnO nanoparticles increased with an increase of the La content up to 0.8 wt% and then decreased. In addition, the properties of other metal dopants such as Al, Ta, Sn, Cu, Cd, Pd, Cr and Mn on the ZnO properties were also investigated [26–33]. However, there have been few reports on the effects of La-doped ZnO nanoparticles on the photocatalytic activity, and none that has reported on the photocatalytic properties of the La-doped ZnO nanoparticles prepared by mechanical milling. Therefore, we have studied and compared the structural, optical and photocatalytic properties of La-doped ZnO nanoparticles prepared by both precipitation and mechanical milling methods.

2. Experimental

The starting materials used in this experiment were analytical grade and used without further purification. Zinc acetate dihydrate ($Zn(CH_3COO)_2 \cdot 2H_2O$) and sodium hydroxide (NaOH) were from Sigma-Aldrich, Germany. Lanthanum chloride hydrate ($LaCl_3 \cdot H_2O$) was from Fluka, Austria. Poly (ethylene glycol)-block-poly (propylene glycol)-block-poly (ethylene glycol) ($PEO_{128}PPO_{54}PEO_{128}$, M.W. 14,400) was from Fluka, France. Zinc oxide (ZnO) was from Fluka, Switzerland, lanthanum oxide (La_2O_3) was from Fluka, China and methylene blue ($C_{16}H_{18}N_3ClS \cdot 2H_2O$) was from UNILAB, Australia.

2.1. The mechanical milling method

Powders were weighed to obtain mixtures of ZnO with 1, 3, 5, 7 and 10 mol% La_2O_3 or equivalent to a stoichiochemistry of $Zn_{1-x}La_xO$ where $x = 0$, 0.01, 0.03, 0.05, 0.07 and 0.10, respectively. The milling was done by a Pulverisette 7 FRITSCH planetary ball mill. Both the vessel and the balls were made from silicon nitride. The ball-to-powder weight ratio was 10:1. The milling speed and milling time were 400 rmp and 15 h, respectively. The mixtures were milled for 10 min, alternating with a stop for 5 min to prevent overheating and to reduce engine wear. After collecting the products, they were annealed in air at 600 °C for 1 h.

2.2. The precipitation method

The 0.01 mol $Zn(CH_3COO)_2 \cdot 2H_2O$ was dissolved in 100 mL distilled water at room temperature by vigorous and continuous stirring. Then, the 1, 3, 5, 7 or 10 mol% $LaCl_3 \cdot H_2O$ was added into each of the zinc precursor solutions. After that, 0.7 mmol $PEO_{128}PPO_{54}PEO_{128}$ was added into the above solutions and stirred until the solutions were clear. Finally, 0.1 mol NaOH dissolved in 100 mL distilled water was added slowly into the $PEO_{128}PPO_{54}PEO_{128}$-modified precursor solutions. The white precipitates that formed were continuously stirred at 60 °C for 1 h before filtering, rinsing with distilled water several times and ethanol, drying at room temperature then finally calcined at 600 °C in air for 1 h.

2.3. Characterizations

The structural and phase formations were identified by an X-ray diffractometer (XRD, X'Pert MPD, PHILIPS). The morphological investigation was carried out by a scanning

electron microscopy (SEM, QUANTA 400, FEI). The diffuse reflectance spectra of the La-doped ZnO nanoparticles were recorded by a UV–vis spectrophotometer (UV–vis 2450, Shimadzu) and the room temperature photoluminescence (PL) spectra of the La-doped ZnO nanoparticles were determined by a luminescence spectrometer (LS/55, Perkin–Elmer).

2.4. The photocatalytic degradation test

The photocatalytic activity of the La-doped ZnO nanoparticles, was evaluated by using methylene blue (MB) as the model at room temperature and pH 6.5, after irradiation with UV light. In a typical procedure, a mixture of 150 mL of 1.5×10^{-5} M MB solution and 150 mg of the La-doped ZnO nanoparticles was stirred for 30 min, to reach adsorption equilibrium in the dark. The mixture was then photoirradiated using three parallel blacklight fluorescent tubes (15 W). 3 mL of the MB solution was collected after irradiation times of 0.5, 1.0, 1.5, 2.0, 2.5 and 3.0 h and centrifuged to separate the powders. The concentrations of the remaining MB solutions were analyzed using a UV–vis spectrophotometer (lambda25, Perkin–Elmer) at 665 nm.

3. Results and discussion

3.1. XRD analysis

In order to investigate the crystal structure, lattice parameters and crystallite sizes of the La-doped ZnO nanoparticles, XRD analysis was used. Fig. 1 shows the XRD patterns of pure ZnO and La-doped ZnO nanoparticles prepared by the precipitation and mechanical milling methods.

For the La-doped ZnO nanoparticles prepared by the precipitation method, the XRD analysis showed that a secondary phase occurred in the XRD pattern when the La content was ≥ 3 mol% (Fig. 1a). The major phase observed in the XRD pattern was the ZnO hexagonal wurtzite structure according to the JCPDS standard card number 36-1451 and the secondary phase observed in the XRD pattern was for La_2O_3. The XRD patterns of the La-doped ZnO nanoparticles prepared by the mechanical milling (Fig. 1 b) were similar to the ZnO powder and were indexed to the pure ZnO hexagonal wurtzite structure according to the JCPDS standard card number 36-1451 when the La content was in a range of 0–7 mol%. An exception was that, a peak of the secondary phase appeared as the La content was doped at 10 mol%. It was evident that different amounts of La can be incorporated into the ZnO lattice produced by different methods even though the La content was first introduced at the same equivalence to the stoichiometry of the $Zn_{1-x}La_xO$ (where $x=0$, 0.01, 0.03, 0.05, 0.07 and 0.10). From the XRD results, it was determined that the La can be more easily incorporated into the ZnO lattice when it was prepared by mechanical milling. This is because the impact

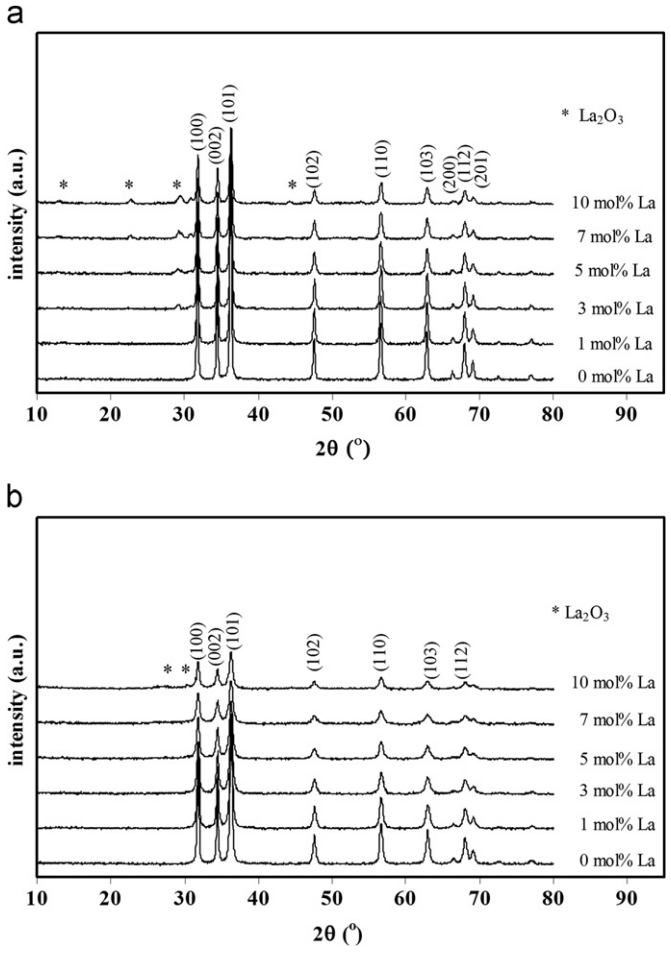

Fig. 1. XRD patterns of La-doped ZnO nanoparticles prepared by different methods (a) precipitation and (b) mechanical milling.

force from the collision process can drive the incorporation of La. A higher intensity of the XRD peaks was observed from the samples prepared by the precipitation method. This indicated a better crystallinity. In this study, the lattice parameters for a and c for the hexagonal wurtzite structure were evaluated from the (100) and (002) planes, respectively through the following relationship [34]:

$$\frac{1}{d_{hkl}^2} = \frac{4}{3}\left[\frac{h^2+hk+k^2}{a^2}\right] + \frac{l^2}{c^2} \quad (1)$$

where d_{hkl} is the lattice spacing of the (hkl) plane and a and c are the lattice parameters. It was observed that the lattice parameters a and c of the La-doped ZnO nanoparticles showed little change but were decreased when compared with the undoped ZnO nanoparticles. Because the ionic radius of the La^{3+} ion (116 pm) is larger than the ionic radius of the Zn^{2+} ion (74 pm), it is more difficult for the La^{3+} to substitute for the Zn^{2+} ion as also occurred in the case of Ce-doped ZnO nanoparticles [35]. This is in good agreement with the Hume-Rothery rules, a substitutional solid solution cannot form, if the atomic radii of the La differ from the Zn by more than 15%. For this reason, the La^{3+} ions prefer to become interstitial in the ZnO lattice where they form a complex with the surface oxygen of the

Table 1
Data from the XRD analysis for the La-doped ZnO nanoparticles prepared by different methods.

Method	La (mol%)	D (nm)	l (nm)	Lattice parameter (nm)		E_g (eV)
				a	c	
Precipitation	0	38.89	0.3737	0.3252	0.5210	3.217
	1	38.61	0.3735	0.3250	0.5207	3.221
	3	37.82	0.3735	0.3249	0.5207	3.220
	5	35.71	0.3735	0.3251	0.5207	3.203
	7	33.61	0.3733	0.3249	0.5205	3.200
	10	27.56	0.3731	0.3247	0.5203	3.196
Mechanical milling	0	37.53	0.3734	0.3249	0.5206	3.156
	1	33.36	0.3731	0.3247	0.5202	3.159
	3	31.28	0.3730	0.3247	0.5200	3.163
	5	29.80	0.3730	0.3247	0.5200	0.169
	7	25.80	0.3728	0.3247	0.5199	3.171
	10	33.35	0.3734	0.3248	0.5206	3.154

ZnO nanoparticles as reported elsewhere [25,35,36], and caused a decrease of the lattice parameter for the La-doped ZnO nanoparticles prepared by the mechanical milling method (Table 1). In a similar way, the lattice parameters of the La-doped ZnO nanoparticles prepared by the precipitation method slightly decreased as a function of the La content. This decrease in the lattice parameters was influenced by the La_2O_3 secondary phase as demonstrated in our previous study [34].

Normally, the width of the diffraction peaks is related to the crystallite size, microstrain and defects such as their stacking faults and dislocations [37]. The crystallite size can be calculated using the Scherrer equation [34]:

$$d = \frac{k\lambda}{\beta \cos\theta} \tag{2}$$

where k is the constant, θ is the Bragg angle of (hkl) reflections, λ is the wavelength of X-rays used and d is the crystallite size.

For the nanoparticles obtained, it was observed that the crystallite size of the La-doped ZnO nanoparticles decreased with an increasing content of La doping except for the ZnO doping with 10 mol% La prepared by the mechanical milling method. In this study, the reduction of the crystallite size can be explained by two possible mechanisms. First, the decrease in the crystallite size of the La-doped ZnO nanoparticles is mainly attributed to the formation of La–O–Zn on the surface of the La-doped ZnO nanoparticles. This can inhibit the crystal growth [25]. The bond length of the La-doped ZnO nanoparticles was calculated to observe the influence of the La doping content via the following equation [37] and the result is tabulated in Table 1.

$$l = \sqrt{\left[\frac{a^2}{3} + \left(\frac{3}{4} - \frac{a^2}{3c^2}\right)^2 c^2\right]} \tag{3}$$

where l is the bond length and a and c are the lattice parameters. The bond length slightly contracts as a function of the La doping content except for the 10 mol% La-doped ZnO nanoparticles prepared by mechanical milling and this result is in good agreement with the crystallite size obtained. Secondly, the decrease in crystallite size as a function of the La content can be explained by the Zener pinning and solute drag effect as reported in Ref. [13].

3.2. Morphological study

The La-doped ZnO nanoparticles obtained by both the precipitation and mechanical milling methods show clusters of agglomerated nanoparticles (Fig. 2). For the La-doped ZnO nanoparticles fabricated by the precipitation method, the particles had agglomerated as shown in Fig. 2(a). In a similar way, the La-doped ZnO nanoparticles milled at 400 rpm for 15 h and then annealed at 600 °C for 1 h produced homogeneous spherical nanoparticles that became agglomerated into the clusters (Fig. 2b). As we know that the nanomaterials are thermodynamically metastable, thus the nanoparticles prefer to associate with one another to form large stable structures in order to reduce the overall surface energy. Obviously, the particle size of the La-doped ZnO nanoparticles prepared by the precipitation method at the same equivalent La doping content is bigger than the particles obtained from mechanical milling. The larger particles can be explained by the Ostwald ripening effect, in which a relatively large particle grows at the expense of the smaller ones. Normally, the Ostwald ripening occurs over a wide range of temperatures and the Ostwald ripening occurs more easily when the particles are dispersed in a solvent. This ripening was encouraged when the aging process occurred at 60 °C for 1 h, when the precipitation method was utilized. In this study, there was a difference between the crystallite and the particle sizes. The reason is well known, as the particle size obtained from the SEM was obtained from the difference

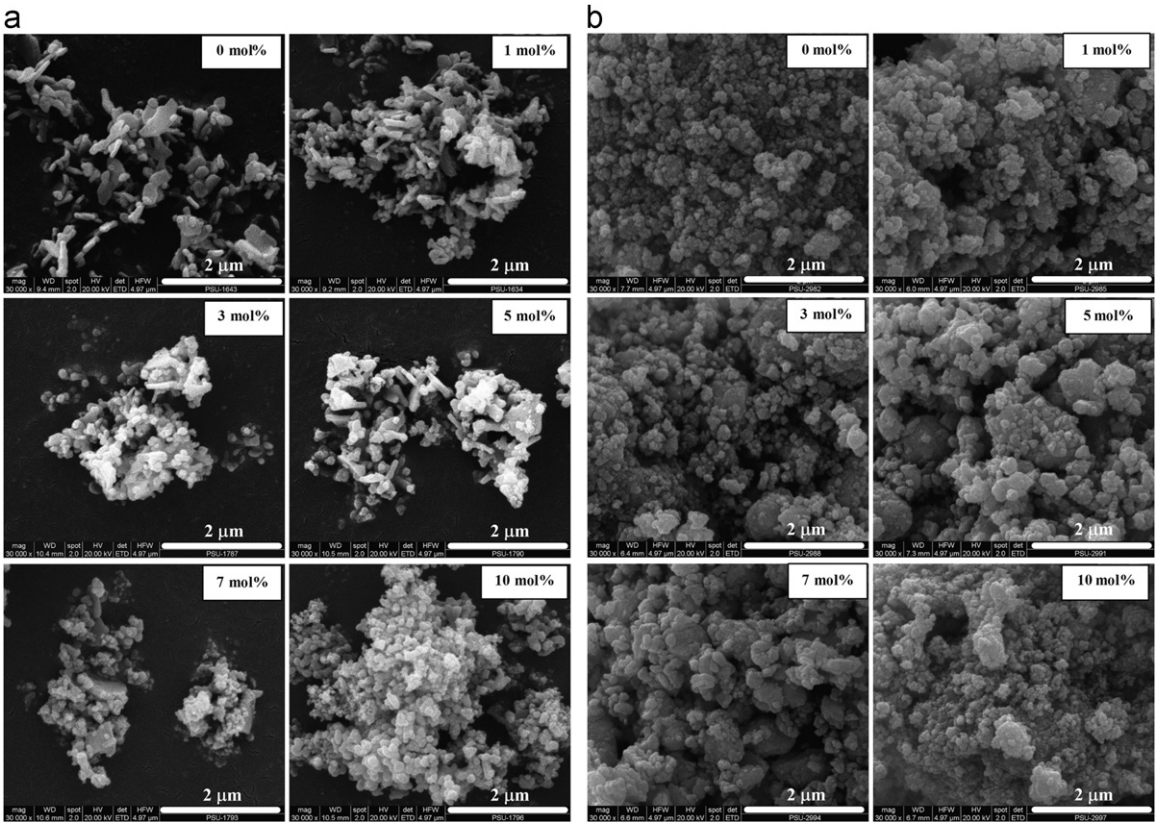

Fig. 2. SEM images of La-doped ZnO nanoparticles prepared by different methods (a) precipitation and (b) mechanical milling.

between the grain boundaries, whereas the crystallite size was obtained from the XRD analysis that was extended to the crystalline region and coherently diffracted the X-ray [15].

3.3. Optical properties

The optical properties are very important parameter to select the materials for use in a particular application. In this study, the band gap energy (E_g) of the La-doped ZnO nanoparticles was evaluated from the plot of $(\alpha E)^2$ versus E when using the data from the transmittance spectra. The absorption coefficient (α) can be calculated from the following relationship [15]:

$$\alpha = \frac{1}{t}\ln\left(\frac{1}{T}\right) \tag{4}$$

where t is the thickness of the samples (0.4 cm) and T is the transmittance. The photon energy (E) was estimated by the relationship [1]:

$$E = \frac{1240}{\lambda} \tag{5}$$

where λ is the wavelength in nanometers. The values of the direct band gap energy were obtained from the linear portion of the plots after extrapolating to zero as shown in Fig. 3 and the results are given in Table 1.

The E_g value shifted to the shorter or longer wavelengths depending upon a number of factors. The shift to the shorter wavelength (blue shift) generally occurred when the particle size decreased [38]. When the particle size was smaller than the Bohr's radius, the blue shift can be explained by the size effect or the effect of quantum confinement [38]. However, the size of all the products in this experiment is beyond the Bohr's radius, thus the change in E_g values might be influenced by other parameters. Based on the result in Table 1, the largest E_g values were obtained from the $Zn_{0.93}La_{0.07}O$ and $Zn_{0.99}La_{0.01}O$ nanoparticles prepared by the mechanical milling and precipitation methods, respectively. The La content was further increased for each method when the secondary phase formed and the E_g values then decreased. Therefore, the increase in the E_g value of the samples can be attributed to an increase in the repulsion between the lowest conduction band edge of the ZnO that originated from the 4s state of the Zn atom and the highest valence band edge from the 2p state of the O atom [4]. In contrast, the formation of the La_2O_3 secondary phase caused a reduction of the E_g value. Therefore, to summarize the E_g value of the La-doped ZnO nanoparticles depended upon a variety of parameters such as the size and presence of the La dopant in different forms. These unique characteristics were influenced by the quality and physical properties of the La-doped ZnO nanoparticles and these were strongly related to the preparation method.

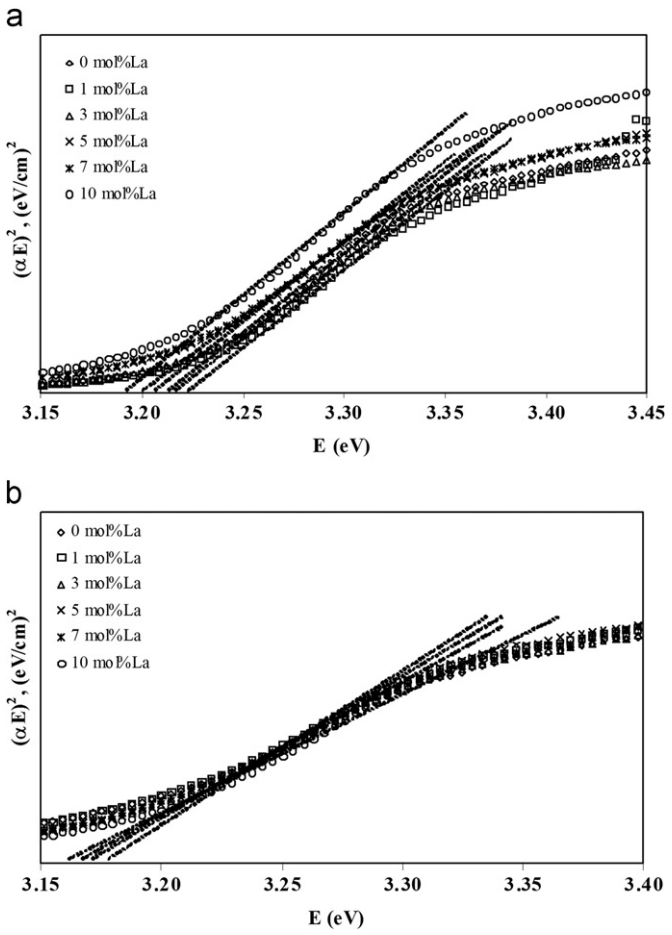

Fig. 3. Plots of $(\alpha E)^2$ versus E for evaluating the E_g value of the La-doped ZnO nanoparticles prepared by different methods (a) precipitation and (b) mechanical milling.

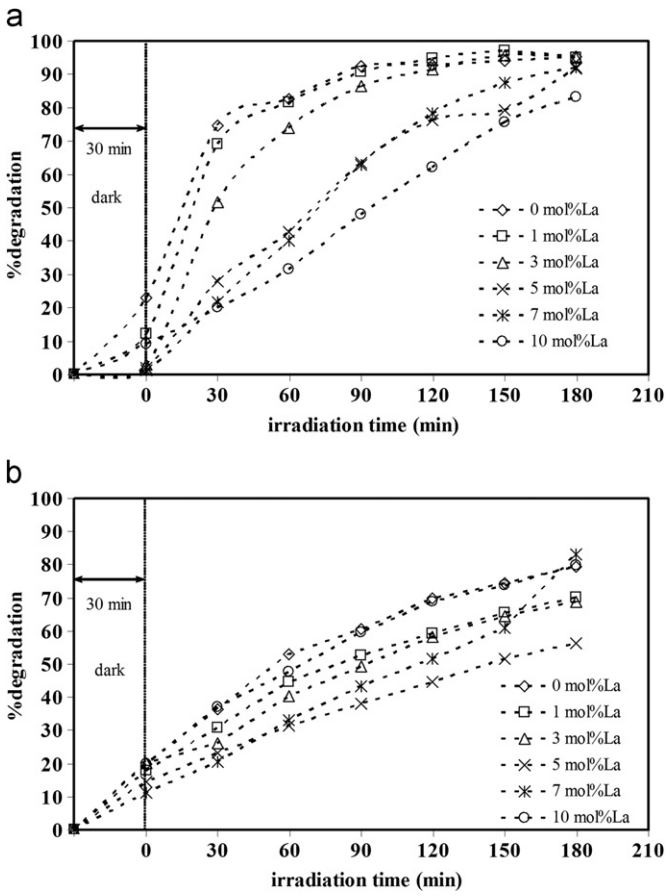

Fig. 4. Photocatalytic degradation of a MB solution for La-doped ZnO nanoparticles prepared by different methods (a) precipitation and (b) mechanical milling.

3.4. Photocatalytic activity

Fig. 4 shows the photocatalytic degradation of an MB solution as a function of the irradiation time on the La-doped ZnO nanoparticles prepared by the precipitation method (Fig. 4(a)) and mechanical milling method (Fig. 4(b)). The photocatalytic efficiency depended on the irradiation time because the MB molecules can become more oxidized with a longer irradiation time. When the samples adsorbed the photons with energy equal to or higher than its band gap energy, the electrons were excited into the conduction band and holes were generated in the valence band. The photogenerated electrons reacted with O_2 or oxygen species to produce superoxide anion radicals ($^{\bullet}O_2^-$) whereas the photogenerated holes react with water molecules to generate the hydroxyl radical ($^{\bullet}OH$). Both these radicals can decompose the MB molecules [19].

For the La-doped ZnO nanoparticles prepared via the precipitation method, 1 mol% La-doped ZnO powders exhibited the highest potential for degradation of MB molecules after irradiating for 2 h, and the degradation efficiency was then constant at about 93% (Fig. 4 a) when the irradiation time was further increased for the ZnO and the ZnO doped with 1 and 3 mol% La. The concentration sequence for the degradation efficiency was 1, 0, 3, 5, 7 and 10 mol% for the La-doped ZnO nanoparticles. This is due to the presence of different amounts of oxygen vacancies [39]. The oxygen vacancies resulted in an increase of the active centers. This improved the photocatalytic activity. In this study, 1 mol% La-doped ZnO nanoparticles had the most oxygen vacancies (Fig. 5a). The photoluminescent spectrometer was used to detect the emission of the samples in the range of 450–800 nm. The emission peak in the visible region occurred from defects in the samples. From this point of view, the 1 mol% La-doped ZnO nanoparticles exhibited the highest intensity, so this sample had the highest degradation efficiency. For the La-doped ZnO nanoparticles prepared through the mechanical milling method, the concentration sequence for the degradation efficiency was 0, 10, 1, 3, 7, and 5 mol% for the La-doped ZnO powders. This can be explained by the amount of oxygen vacancies (Fig. 5 b).

When considering the La-doped ZnO nanoparticles prepared by different methods, the La-doped ZnO nanoparticles prepared by the precipitation method showed better photocatalytic activity than that of the La-doped ZnO nanoparticles prepared by the mechanical milling method.

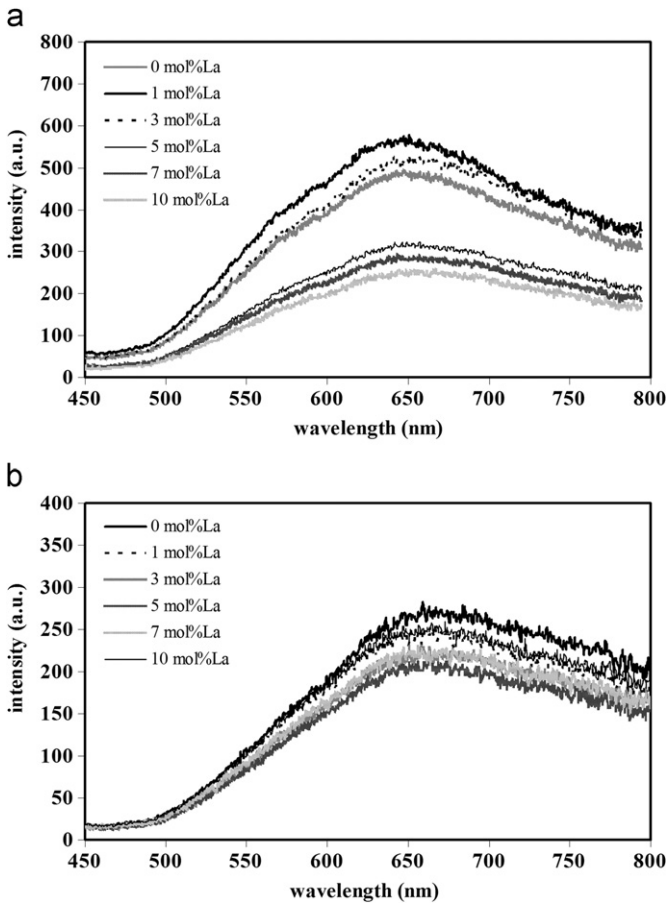

Fig. 5. Room temperature photoluminescence spectra of the La-doped ZnO nanoparticles prepared by different methods (a) precipitation and (b) mechanical milling.

This is because the La-doped ZnO nanoparticles prepared by the precipitation method occupied more oxygen vacancies that can be observed from Fig. 5. The La-doped ZnO nanoparticles prepared by the precipitation method showed a higher intensity in the visible region. As we know, the photocatalytic activity depended upon the specific surface area of catalyst, however, many research workers [40,41] reported that other parameters such as morphology, crystalline structure, defect and impurity contents might affect in a greater way than the specific surface area.

In this study, the Langmuir–Hinshelwood (L–H) model was used to describe the heterogeneous photocatalytic reaction between the La-doped ZnO nanoparticles and the MB solution. The L–H kinetic equation is [42]:

$$r = \frac{kK[C]}{1+K[C]} \tag{6}$$

where r is the degradation rate for MB, K is the adsorption coefficient for MB on the surface of the La-doped ZnO nanoparticles, k is the surface pseudo-first-order rate constant and C is the concentration of the MB solution. If the adsorption coefficient on the surface of the La-doped ZnO nanoparticles is too small, so that $1 \gg K[C]$, and the L–H kinetic equation reduces to the following simple first-order kinetic law:

$$r = k^*[C] \tag{7}$$

where k^* is the first-order rate constant and is equal to kK.

The plot of $\ln(C_0/C)$ versus the irradiation times is presented in Fig. 6 in order to evaluate the first-order rate constant shown in Table 2.

The fastest degradation rate for the decomposition of the MB solution was obtained from the 1 mol% La-doped ZnO nanoparticles when the ZnO nanoparticles were prepared by precipitation and mechanical milling methods, respectively. This can be explained by the more active centers of the powders.

4. Conclusions

$Zn_{1-x}La_xO$ (where $x=0$–0.07) and $Zn_{1-x}La_xO$ (where $x=0$–0.01) nanoparticles can be produced by the mechanical milling and precipitation methods, respectively. More La can be incorporated into the ZnO structure when it was prepared by mechanical milling compared to the

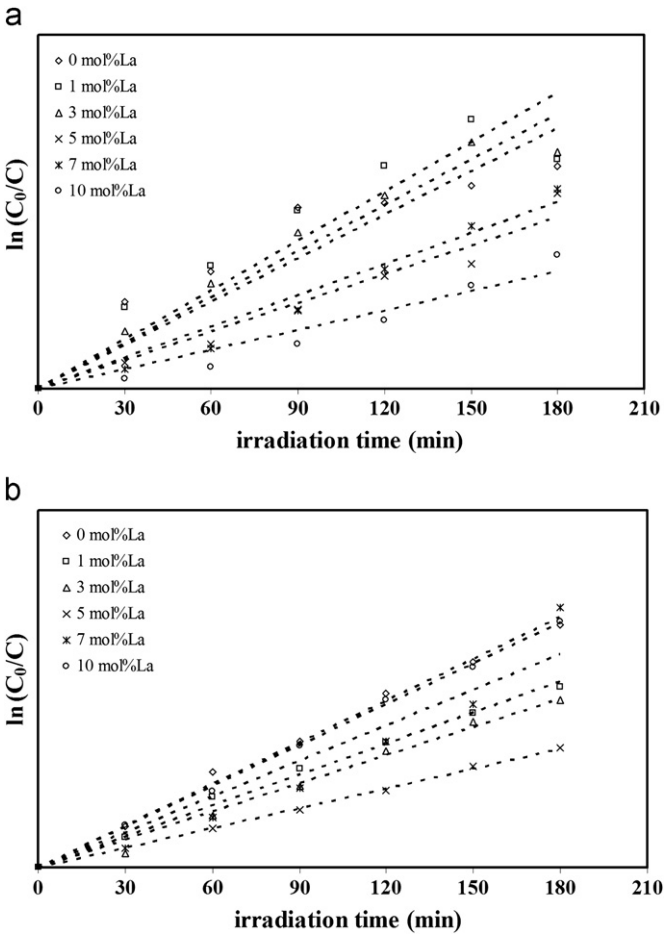

Fig. 6. Kinetics of the MB degradation catalyzed by the La-doped ZnO nanoparticles prepared by different methods (a) precipitation and (b) mechanical milling.

Table 2
Effect of the La-doped ZnO nanoparticles prepared by different methods on the rate constants for degradation of MB.

Method	La (mol%)	k^* (min^{-1})	Photodegradation rate at 2 h ($M\ min^{-1}$)	R^2
Precipitation	0	0.0184	1.11×10^{-8}	0.8084
	1	0.0208	8.86×10^{-9}	0.8473
	3	0.0196	1.40×10^{-8}	0.9472
	5	0.0122	2.39×10^{-8}	0.9600
	7	0.0133	2.39×10^{-8}	0.9694
	10	0.0083	2.61×10^{-8}	0.9352
Mechanical milling	0	0.0078	2.70×10^{-8}	0.9942
	1	0.0058	2.71×10^{-9}	0.9947
	3	0.0053	2.53×10^{-8}	0.9889
	5	0.0037	2.35×10^{-8}	0.9988
	7	0.0066	3.67×10^{-8}	0.9178
	10	0.0076	2.73×10^{-8}	0.9984

precipitation method because of the extra driving force provided by the milling collision process. La_2O_3/ZnO composite nanoparticles were formed when a higher La amount was used in each method. The crystallite size and particle size of the samples prepared by the precipitation method were larger than the samples obtained by the mechanical milling method because of the growth of the particle via the Ostwald ripening mechanism. The widest E_g value of about 3.171 eV was obtained for the $Zn_{0.93}La_{0.07}O$ nanoparticles prepared by the mechanical milling method whilst the widest E_g value of about 3.221 eV was obtained for the $Zn_{0.99}La_{0.01}O$ nanoparticles prepared by the precipitation method. The presence of a La_2O_3 secondary phase produced a decrease in the E_g value for samples prepared by both techniques. For mechanical milling method, ZnO nanoparticles produced the highest photocatalytic degradation of methylene blue, while the $Zn_{0.99}La_{0.01}O$ powder prepared by the precipitation method showed the highest efficiency. This was attributed to the oxygen vacancies.

Acknowledgment

This work has been supported by the Thailand Research Fund (TRF) under the contract number MRG5480072, Office of the Higher Education Commission and Prince of Songkla University. The authors would like to acknowledge the National Nanotechnology Center (NANOTEC), NSTDA, Ministry of Science and Technology, through its program of Center of Excellence Network at PSU and the Center of Excellence for Innovation in Chemistry (PERCH – CIC), Office of the Higher Education Commission, Ministry of Education and the authors would like to thank Dr. Brian Hodgson for his assistance with the English.

References

[1] S. Suwanboon, P. Amornpitoksuk, N. Muensit, Dependence of photocatalytic activity on structural and optical properties of nanocrystalline ZnO powders, Ceramics International 37 (2011) 2247–2253.
[2] M.M. Mikhailov, V.V. Neshchimenko, N.V. Dedov, L. Chundong, H. Shiyu, Proton and electron irradiation induced changes in the optical properties of ZnO pigments modified with ZrO_2 and Al_2O_3 nanopowders, Journal of Surface Investigation: X-ray, Synchrotron and Neutron Techniques 5 (2011) 1152–1161.
[3] V.I. Kushnirenko, I.V. Markevich, T.V. Zashivailo, Acceptors related to group I elements I ZnO ceramics, Journal of Luminescence 132 (2012) 1953–1956.
[4] P. Amornpitoksuk, S. Suwanboon, S. Sangkanu, A. Sukhoom, N. Muensit, Morphology, photocatalytic and antibacterial activities of radial spherical ZnO nanorods controlled with a diblock copolymer, Superlattices and Microstructures 51 (2012) 103–113.
[5] M. Vishwas, K. Narasimha Rao, K.V. Arjuna Gowda, R.P.S. Chakradhar, Influence of Sn doping on structural, optical and electrical properties of ZnO thin films prepared by cost effective sol–gel process, Spectrochimica Acta, Part A: Molecular and Biomolecular Spectroscopy 95 (2012) 423–426.
[6] U. Sirimahachai, S. Phongpaichit, S. Wongnawa, Evaluation of bactericidal activity of TiO_2 photocatalysts: a comparative study of laboratory-made and commercial TiO_2 samples, Songklanakarin Journal of Science and Technology 31 (2009) 517–525.
[7] S.D. Perera, R.G. Mariano, K. Vu, N. Nour, O. Seitz, Y. Chabal, K.J. Balkus Jr, Hydrothermal synthesis of grapheme-TiO_2 nanotube composites with enhanced photocatalytic activity, Catalysis 2 (2012) 949–956.
[8] D. Zhang, Photocatalytic applications of Au-deposited on TiO_2 nanocomposite catalyst in dye degradation via photoreduction, Russian Journal of Physical Chemistry A 86 (2012) 498–503.
[9] C. Chen, J. Liu, P. Liu, B. Yu, Investigation of photocatalytic degradation of methyl orange by using nano-sized ZnO catalysts, Advances in Chemical Engineering and Science 1 (2011) 9–14.
[10] V. Houskova, V. Stengl, S. Bakardjieva, N. Murafa, A. Kalendova, F. Oplustil, Zinc oxide prepared by homogeneous hydrolysis with thioacetamide, its destruction of warfare agent and photocatalytic activity, The Journal of Physical Chemistry A 111 (2007) 4215–4221.
[11] Y.S. Chang, Y.H. Chang, I.G. Chen, G.J. Chen, Y.L. Chai, T.H. Fang, S. Wu, Synthesis, formation and characterization of $ZnTiO_3$ ceramics, Ceramics International 30 (2004) 2183–2189.
[12] N.S. Sabri, A.K. Yahya, M.K. Talari, Emission properties of Mn doped ZnO nanoparticles prepared by mechanochemical processing, Journal of Luminescence 132 (2012) 1735–1739.
[13] S. Suwanboon, P. Amornpitoksuk, P. Bangrak, Synthesis, characterization and optical properties of $Zn_{1-x}Ti_xO$ nanoparticles prepared via a high-energy ball milling technique, Ceramics International 37 (2011) 333–340.

[14] N. Ye, C.C. Chen, Investigation of ZnO nanorods synthesized by a solvothermal method, Optical Materials 34 (2012) 753–756.
[15] S. Suwanboon, Structural and optical properties of nanocrystalline ZnO powder from sol–gel method, Science Asia: Journal of the Science Society of Thailand 34 (2008) 31–34.
[16] N. Samaele, P. Amornpitoksuk, S. Suwanboon, Effect of pH on the morphology and optical properties of modified ZnO particles by SDS via a precipitation method, Powder Technology 203 (2010) 243–247.
[17] S. Suwanboon, P. Amornpitoksuk, A. Sukolrat, Dependence of optical properties on doping metal, crystallite size and defect concentration of M-doped ZnO nanopowders (M=Al, Mg, Ti), Ceramics International 37 (2011) 1359–1365.
[18] C. Suryanarayana, Mechanical alloying and milling, Progress in Materials Science 46 (2011) 1–184.
[19] P. Amornpitoksuk, S. Suwanboon, S. Sangkanu, A. Sukhoom, N. Muensit, J. Baltrusaitis, Synthesis, characterization, photocatalytic and antibacterial activities of Ag-doped ZnO powders modified with a diblock copolymer, Powder Technology 219 (2012) 158–164.
[20] H. Benhebal, M. Chaib, A. Leonard, S.D. Lambert, M. Crine, Photodegradation of phenol and benzoic acid by sol–gel synthesized alkali metal-doped ZnO, Materials Science in Semiconductor Processing 15 (2012) 264–269.
[21] R. He, R.K. Hocking, T. Tsuzuki, Co-doped ZnO nanopowders: location of cobalt and reduction in photocatalytic activity, Materials Chemistry and Physics 132 (2012) 1035–1040.
[22] C. Xu, L. Cao, G. Su, W. Liu, X. Qu, Y. Yu, Preparation, characterization and photocatalytic activity of Co-doped ZnO powders, Journal of Alloys and Compounds 497 (2010) 373–376.
[23] J.B. Zhong, J.Z. Li, Y. Lu, X.Y. He, J. Zeng, W. Hu, Y.C. Shen, Fabrication of Bi^{3+}-doped ZnO with enhanced photocatalytic performance, Applied Surface Science 258 (2012) 4929–4933.
[24] A.B. Patil, K.R. Patil, S.K. Pardeshi, Ecofriendly synthesis and solar photocatalytic activity of S-doped ZnO, Journal of Hazardous Materials 183 (2010) 315–323.
[25] S. Anandan, A. Vinu, K.L.P. Sheeja Lovely, N. Gokulakrishnan, P. Srinivasu, T. Mori, V. Murugesan, V. Sivamurugan, K. Ariga, Photocatalytic activity of La-doped ZnO for the degradation of monocrotophos in aqueous suspension, Journal of Molecular Catalysis A: Chemical 266 (2007) 149–157.
[26] K.C. Hsiao, S.C. Liao, Y.J. Chen, Synthesis, characterization and photocatalytic property of nanostructured Al-doped ZnO powders prepared by spray pyrolysis, Materials Science and Engineering, A: Structural Materials: Properties, Microstructure and Processing 447 (2007) 71–76.
[27] J.Z. Kong, A.D. Li, H.F. Zhai, Y.P. Gong, H. Li, D. Wu, Preparation, characterization of the Ta-doped ZnO nanoparticles and their photocatalytic activity under visible-light illumination, Journal of Solid State Chemistry 182 (2009) 2061–2067.
[28] X. Jia, H. Fan, M. Afzaai, X. Wu, P. O'Brien, Solid state synthesis of tin-doped ZnO at room temperature: characterization and its enhanced gas sensing and photocatalytic properties, Journal of Hazardous Materials 193 (2011) 194–199.
[29] R. Mohan, K. Krishnamoorthy, S.J. Kim, Enhanced photocatalytic activity of Cu-doped ZnO nanorods, Solid State Communications 152 (2012) 375–380.
[30] C. Karunakaran, A. Vijayabalan, G. Manikandan, Photocatalytic and bactericidal activities of hydrothermally synthesized nanocrystalline Cd-doped ZnO, Superlattices and Microstructures 51 (2012) 443–453.
[31] J.B. Zhong, J.Z. Li, X.Y. He, J. Zeng, Y. Lu, W. Hu, K. Lin, Improved photocatalytic performance of Pd-doped ZnO, Current Applied Physics 12 (2012) 998–1001.
[32] C. Wu, L. Shen, Y.C. Zhang, Q. Huang, Solvothermal synthesis of Cr-doped ZnO nanowires with visible light-driven photocatalytic activity, Materials Letters 65 (2011) 1794–1796.
[33] R. Ullah, J. Dutta, Photocatalytic degradation of organic dyes with manganese-doped ZnO nanoparticles, Journal of Hazardous Materials 156 (2008) 194–200.
[34] S. Suwanboon, P. Amornpitoksuk, Preparation and characterization of nanocrystalline La-doped ZnO powders through a mechanical milling and their optical properties, Ceramics International 37 (2011) 3515–3521.
[35] M. Yousefi, M. Amiri, R. Azimirad, A.Z. Moshfegh, Enhanced photoelectrochemical activity of Ce doped ZnO nanocomposite thin films under visible light, Journal of Electroanalytical Chemistry 661 (2011) 106–112.
[36] G. Srinivasan, R.T. Rajendra Kumar, J. Kumar, Li doped and undoped ZnO nanocrystalline thin films: a comparative study of structural and optical properties, Journal of Sol–Gel Science and Technology 43 (2007) 171–177.
[37] A. George, S.K. Sharma, S. Chawla, M.M. Malik, M.S. Qureshi, Detailed of X-ray diffraction and photoluminescence studied of Ce doped ZnO nanocrystals, Journal of Alloys and Compounds 509 (2011) 5942–5946.
[38] S. Suwanboon, P. Amornpitoksuk, A. Haidoux, J.C. Tedenac, Structural and optical properties of undoped and aluminium doped zinc oxide nanoparticles via precipitation method at low temperature, Journal of Alloys and Compounds 462 (2008) 335–339.
[39] L. Song, S. Zhang, X. Wu, Q. Wei, Controllable synthesis of hexagonal, bullet-like ZnO microstructures and nanorod arrays and their photocatalytic property, Industrial and Engineering Chemistry 51 (2012) 4922–4926.
[40] H. Wang, C. Xie, W. Zhang, S. Cai, Z. Yang, Y. Gui, Comparison of dye degradation efficiency using ZnO powders with various size scales, Journal of Hazardous Materials 141 (2007) 645–652.
[41] G. Colón, M.C. Hidalgo, J.A. Navío, E. Pulido Melián, O. González Díaz, J.M. Doña Rodríguez, Highly photoactive ZnO by amine capping-assisted hydrothermal treatment, Applied Catalysis, B: Environmental 83 (2008) 30–38.
[42] C. Karunakaran, B. Naufal, P. Gomathisankar, Efficiency photocatalytic degradation of salicylic acid by bactericidal ZnO, Journal of the Korean Chemical Society 56 (2012) 108–114.